types de domaines ordonnés, de grande extension, équireprésentés dans le cristal. Un type de domaine contient, pour chaque variété d'anions, deux orientations *A* pour une orientation *B*, l'autre deux orientations *B* pour une orientation *A*. Il est remarquable qu'une analyse structurale classique des composés $NiSiF_6.6H_2O$ et $ZnSiF_6.6H_2O$ (Ray, Zalkin & Templeton, 1973) ait conduit à des proportions identiques pour les deux orientations d'octaèdres (deux orientations *A* pour une orientation *B*), dans le cas d'une répartition désordonnée de ces octaèdres ($R\bar{3}$). La structure présentée ($P\bar{3}$) pour $MgSiF_6.6H_2O$ peut être regardée comme une structure antiphasée périodique, à période entière [$2M = 3d_{(101)}$], fondée sur la structure ordonnée monoclinique de basse température ($P2_1/c$).

Cette manière d'envisager la structure du fluosilicate de magnésium devait nous permettre de traiter le cas du fluosilicate de fer dans toutes ses particularités (taches de surstructure d'extension variable à indices non strictement entiers). Cette étude en voie d'achèvement fera l'object d'une prochaine publication.

Nous remercions R. Saint-James pour la préparation d'échantillons, A. Hardy pour sa collaboration à la mesure des intensités diffractées et P. Pério avec qui nous avons eu des fructueuses discussions.

Références

HAMILTON, W. (1962). *Acta Cryst.* **15**, 353–360.
JEHANNO, G. & VARRET, F. (1975). *Acta Cryst.* A**31**, 857–858.
KODERA, E., TORRI, A., OSAKI, K. & WATANABE, T. (1972). *J. Phys. Soc. Jpn*, **32**, 863.
RAY, S. (1972). Symposium on Crystallography, Bombay.
RAY, S., ZALKIN, A. & TEMPLETON, D. H. (1973). *Acta Cryst.* B**29**, 2741–2747.
SYOYAMA, S. & OSAKI, K. (1972). *Acta Cryst.* B**28**, 2626–2627.
TOURNARIE, M. (1969). *J. Phys.* (*Paris*), **10**, 737.
VARRET, F., DANON, J., IMBERT, P. & JEHANNO, G. (1974). *J. Phys.* (*Paris*), *Colloq.* C1, supplément au n° 1, **35**, C1–87.

Acta Cryst. (1979). A**35**, 916–923

The Direct Identification of Stacking Sequences in Silicon Carbide Polytypes by High-Resolution Electron Microscopy

BY N. W. JEPPS

Department of Metallurgy and Materials Science, University of Cambridge, Pembroke Street, Cambridge CB2 3QZ, England

DAVID J. SMITH

EM Section, Old Cavendish Laboratory, University of Cambridge, Free School Lane, Cambridge CB2 3RQ, England

AND T. F. PAGE

Department of Metallurgy and Materials Science, University of Cambridge, Pembroke Street, Cambridge CB2 3QZ, England

(*Received* 4 *April* 1979; *accepted* 15 *May* 1979)

Abstract

Lattice imaging with tilted illumination at the 2·5 Å level has been used for the direct determination of stacking sequences in silicon carbide polytypes by observation of electron micrographs. The method employed is first demonstrated by observations of the common short-period polytypes 3*C*, 4*H*, 15*R* and 6*H*, and is then used to reveal the stacking sequences in the polytypes 9*R* and 129*R*, neither of which appear to have been reported previously. Stacking sequences in disordered and faulted materials have also been characterised.

1. Introduction

Silicon carbide exists as a number of different structural types, commonly called polytypes, which are based on variations of a one-dimensional stacking sequence (Baumhauer, 1912; Ramsdell, 1947; Verma & Krishna, 1966; Shaffer, 1969). X-ray diffraction can be

0567-7394/79/060916-08$01.00

used to examine some bulk aspects of the polytypes (*e.g.* Verma & Krishna, 1966) but is not suitable for the study of more complicated sequences, or when fine-scale structural variations such as stacking faults occur. Electron diffraction and electron microscopy have also been applied to the structure determination of long-period polytypes (Sato, Shinozaki & Yessik, 1974; Yessik, Shinozaki & Sato, 1975; Dubey & Singh, 1978). However, because of limited resolution, identification of detailed stacking sequences within the long-period structures necessitated trial structure factor calculations based on the small number of possible variants.

Our recent observations with high-resolution lattice imaging at the 2·5 Å level with tilted-beam illumination (Smith, Jepps & Page, 1978) established that essentially one-dimensional information about individual stacking sequences was directly obtainable. The technique has since been applied to observations of a variety of silicon carbide polytypes and it has been possible to identify directly the detailed stacking sequence in longer-period polytypes, and around the vicinity of stacking faults, without recourse to any confirmatory calculations based on postulated trial structures.

The present communication describes these observations and the method of interpretation in detail. Calculations with *n*-beam dynamical diffraction theory (Cowley & Moodie, 1957; Goodman & Moodie, 1974) to confirm the validity of the interpretations will be reported elsewhere. However, the experience gained from observations of the common, short-period, polytypes such as $6H$ and $15R$, which are the basic building blocks of the larger-period polytypes, indicates that such calculations are not normally necessary.

2. Structure

Silicon carbide structures consist of primary coordination tetrahedral units of Si and C atoms, these tetrahedra being stacked in positions analogous to those occupied by spheres in close-packed structures and linked through their apices to form a tetrahedral, covalently bonded, polar structure. Two stacking operations are possible, namely, translations of adjacent layers with and without rotations of π, giving, in extreme cases, the zinc blende cubic structure, or the wurtzite hexagonal structure. The opportunity for polytypism is introduced by allowing a mixture of hexagonal and cubic stacking to repeat in one dimension. Tetrahedral models of the four most common polytypes ($3C$, $4H$, $15R$, $6H$)* are shown in Fig. 1, these four structures being the basic units of many of the larger polytypes. Beside each model the stacking sequence is shown. The sequence of tetrahedral layers may be visualised in the models by considering the resulting sequence of non-basal-plane faces. Primarily, the stacking sequence can be identified uniquely if both the arrangement and orientation of the individual tetrahedra can be established. However, such information can also be determined by examination of the appearance of prominent non-basal planes within the structure and this consideration relaxes the requirement for spatial resolution of the tetrahedra or the atomic arrangements themselves. Consider the case of $6H$ (space group $P6_3mc$) with a structure $A'BCAB'C'A'$.* The tetrahedral faces form a zig-zag in the c direction with three layers in one orientation with faces lying on the $\{10\bar{1}2\}$ planes, for example, followed by three layers rotated by π, the corresponding tetrahedral faces of which lie on the $\{10\bar{1}\bar{2}\}$ planes. In all structures similar planes exist which allow visualisation of the stacking sequence.

3. Experimental details

The materials used in these studies were prepared as described previously (Sawyer & Page, 1978; Smith, Jepps & Page, 1978). Observations were made with a JEM-120CX and a high-resolution goniometer holder. The resolution required for obtaining two-dimensional

* The notation $3C$, $6H$ *etc.* is attributed to Ramsdell (1947). It may be used to describe all polytypes; the number denotes the number of layers in one unit cell and the letter (H,C,R) denotes the Bravais-lattice type (hexagonal, cubic, rhombohedral).

* The structure of any polytype may be represented by a modified form of the ABC notation (used for close-packed structures), a dash being added to differentiate between tetrahedral sheets in the same spatial position but rotated by π (Smith, Jepps & Page, 1978).

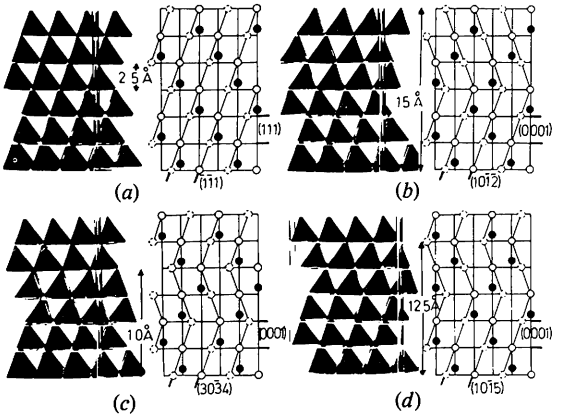

Fig. 1. Structural models, with corresponding stacking sequence diagrams, for various SiC polytypes, namely: (*a*) $3C$ viewed along $\langle 1\bar{1}0\rangle$, (*b*) $6H$ viewed along $\langle 1\bar{2}10\rangle$, (*c*) $4H$ viewed along $\langle 1\bar{2}10\rangle$, (*d*) $15R$ viewed along $\langle 1\bar{2}10\rangle$. Only those tetrahedral face planes in the zone of the viewing direction are shown on the diagrams. All the Si atomic positions are shown (those in the plane of the plan as open circles, those above and below as closed circles), but only those C positions (filled circles) in the plane of the plan have been included.

axial projections of the atomic structure was beyond the capability of the microscope. However, with tilted illumination and careful choice of operating conditions, information about the stacking sequence could be obtained from the behaviour of the lattice fringes of 2·518 Å periodicity, which correspond to the spacing between successive layers. With an electron-optical magnification of up to 700 000× available, these lattice fringes could be observed directly on the fluorescent screen when a pointed tungsten filament was used as the electron source. The unit-cell length of long-period polytypes, together with the spacings of any subperiod structure, can also be measured with a high degree of accuracy as multiples of this 2·518 Å stacking periodicity.

4. The method of direct structure determination

The objective of the present study has been to explore the possibilities for, and limitations of, using high-resolution lattice imaging techniques to obtain direct and unambiguous identification of layer-by-layer stacking sequences in silicon carbide polytypes. The use of selected-area diffraction alone to identify structures is clearly inadequate since fine-scale phase mixtures will produce overlapping patterns. Further, double diffraction occurs increasingly in thicker specimens yielding unexpected intensity in space-group-absent reflections. In thin specimens, tilted-beam lattice imaging using reflections corresponding to the individual tetrahedral layers [*e.g.* $(111)_{3C}$, $(0006)_{6H}$, *etc.*] simply show parallel fringes of ~2·5 Å spacing, without providing any information regarding the stacking operations between layers, so that unambiguous polytype identification is still not possible. Sufficient double diffraction occurs in thicker specimens, in some reciprocal-lattice sections [*e.g.* $(11\bar{2}0)$ for the α-polytypes], to enable rows of systematic space-group-absent reflections to occur, one of which always corresponds to the lattice repeat along the stacking directions [*e.g.* $(0001)_{6H}$, $(0001)_{4H}$, $(0003)_{15R}$, *etc.*]. Although lattice imaging under these conditions may allow this aspect to be imaged alone, or superposed on the fundamental layer fringes, this simply confirms the order of the polytype without isolating a particular stacking sequence in those cases where ambiguity is possible (*e.g.* *C'ABCB'A'C'* or *C'ABA'C'AC'* *etc.* for 6*H*, and more diverse for higher order cases). Also, while stacking faults may be revealed in such images as either local intensity changes and/or changes in separation of the unit-cell spacing fringes (*e.g.* the ~15 Å fringes for 6*H*), fault characterization in terms of stacking details is again precluded. Clearly a different approach is necessary if stacking sequence information is to be obtained directly in lattice images. This must involve consideration of the use of other reflections for lattice imaging.

Examination of the structural model (Fig. 1*a,b,c,d*) reveals those tetrahedral face planes which allow the stacking sequences to be visualised. The reticular density on these planes varies according to the stacking sequence. For 6*H*, for example, the $(10\bar{1}2)$ plane has a high reticular density in one half of the 6*H* cell, whilst $(10\bar{1}\bar{2})$ takes on a similar appearance in the other half.* Without calculation, it seems reasonable to suppose that the diffracted intensity from $(10\bar{1}2)$ will show variation on this scale, and thus lattice imaging with both $10\bar{1}2$ and $10\bar{1}\bar{2}$ simultaneously should reveal the alternate zig-zag nature of this pair of plane stacks. While these tetrahedral face reflections occur in all polytypes where stacking operations occur in units of three (*e.g.* 6*H*, 3*C*, *etc.*), they are systematically absent in other polytypes (*e.g.* 4*H*, 15*R*, *etc.*). However, in these cases, other $10\bar{1}l$ reflections show similar structural variations with stacking sequence (and hence expected intensity variations).† Lattice images with these $10\bar{1}l$ reflections should be capable of showing the changes in the stacking sequence as chevrons of varying angles to **c**. Such images, either viewed together with images of the stack itself or as crossed lattice images produced simultaneously with the stack, should be an ideal means of revealing the stacking sequence directly, removing all possible ambiguities.

4.1. *Structures with allowed tetrahedral face reflections*

Preliminary investigations were made of both 6*H* and twinned 3*C* silicon carbide structures where the contrast observed in the lattice fringe images from the tetrahedral face reflections can be simply compared with the behaviour expected from structural models. In both cases, individual grains from polycrystalline samples were oriented so that the optic axis was parallel to one of the tetrahedral edges (*i.e.* $\langle 1\bar{1}0\rangle_{3C}$; $\langle 1\bar{2}10\rangle_{6H}$) resulting in diffraction patterns containing the tetrahedral face reflections 111_{3C}, $\bar{1}\bar{1}1_{3C}$, $\underline{11\bar{1}}_{3C}$ *etc.* and 0006_{6H}, $10\bar{1}2_{6H}$, $10\bar{1}\bar{2}_{6H}$ *etc.* Figs. 2(*a*) and (*b*) show indexed diffraction patterns from the 6*H* and twinned 3*C* polytypes in this orientation and Fig. 2(*c*) shows lattice fringes from a region of a 6*H*/3*C* interface; the different stacking sequences are clearly resolved. In all cases, the image contrast and geometry is precisely that

* For 6*H*, structure factor calculations show that sub-unit-cell diffracted intensity variations with stacking sequence should occur for $10\bar{1}l$ when $l = \pm 2$ or ± 4 *etc.* but not for $l = 1, 3, 5$ *etc.* This not only leads to the range of equivalent aperture/optic axis positions mentioned in §6 but also implies that the effect of including these latter beams in the aperture is simply to add to the image background at the optimum defocus.

† For 15*R*, $101l$ shows the expected behaviour for $l = \bar{1}\bar{0}, \bar{4}, 5$ and 11 *etc.*, other reflections showing little sub-unit-cell variation (while for 4*H*, $l = \pm 1$). The corresponding interplanar spacings vary with l around ~2·5 Å.

anticipated from structural models allowing the stacking sequence to be followed through individual tetrahedral layers.

4.2. *Structures with absent tetrahedral face reflections*

Those planes corresponding to the tetrahedral faces give the simplest structural realisation of the stacking operations but similar changes in reticular density occur with other sets of structural planes. These would be expected to show orientation change effects in lattice fringe images similar to those described in §4.1.

In both $15R$ and $4H$, tetrahedral face reflections are absent. Figs. 3(*a*) and (*b*) show indexed diffraction patterns from these polytypes. In $15R$, one tetrahedral reflection in this reciprocal-lattice plane is always present, namely 1015, the other, $10\bar{1}5$, being absent due to the rhombohedral cell. Examination of the $(10\bar{1}\bar{4})$ plane, however, reveals that the reticular density varies in a similar way to that of the $(10\bar{1}5)$ plane. Therefore lattice imaging using the $10\bar{1}\bar{4}$ reflection together with $10\bar{1}5$ and the transmitted beam is expected to show fringes with intensity variations according to stacking sequence. Figs. 3(*c*) and (*d*) show tilted-beam lattice fringes from a region of $15R$ with the aperture positions as shown on the diffraction pattern. The sequence of three layers in one orientation followed by two layers in a rotation-twin-related orientation is clearly seen in Fig. 3(*d*).

In $4H$ all tetrahedral face reflections are absent. Consideration of variations of local structure factors reveals, however, that the $10\bar{1}1$ and $10\bar{1}\bar{1}$ reflections may be used to obtain information about the stacking sequence. Figs. 3(*e*) and (*f*) show lattice fringes of the $4H$ structure. Fig. 3(*e*) reveals the (0004) planes and Fig. 3(*f*) enables the stacking operations between each layer to be followed as a chevron of $(10\bar{1}1)$ and $(10\bar{1}\bar{1})$ planes, each set of fringes having greater intensity in those regions of the cell where the reticular density is highest. In all cases where tetrahedral face reflections are absent, lattice fringes produced with other reflections will, because of the diffraction geometry, have different angular relationships. It must therefore be stressed that these fringes do not show tetrahedral positions but only reveal stacking operators.

5. The direct determination of stacking sequences

The use of tilted-beam lattice imaging techniques was shown in the previous section to resolve, reliably and unambiguously, stacking variations at single plane level in the short-period polytypes, regardless of the order of stacking involved. This section presents results obtained with these techniques and includes the identification of a new polytype ($129R$), the possible recognition of a new intermediate structure (tentatively $9R$) and the detailed characterisation of stacking sequences in regions where considerable disorder is occurring.

The micrographs of Figs. 4(*a*) and (*b*) are from a long-period polytype. Observation of its diffraction pattern suggests that it is $129R$. The 000*l* type tilted-beam lattice fringes with 2·518 Å spacing of Fig. 4(*a*) can be used to provide a convenient length calibration. Further from the foil edge, where the double diffraction effects become stronger, there is a modulation of intensity across much of the material with a period of $6 \times 2{\cdot}518 \simeq 15$ Å, which is the unit-cell length of the $6H$ polytype. This suggests that much of the stacking of the polytype may be based on that of the $6H$ polytype, but without tilting the incident beam in the perpendicular direction, the particular stacking sequence cannot be resolved. Careful observation and measurement of the lattice fringes in Fig. 4(*b*) in fact show that

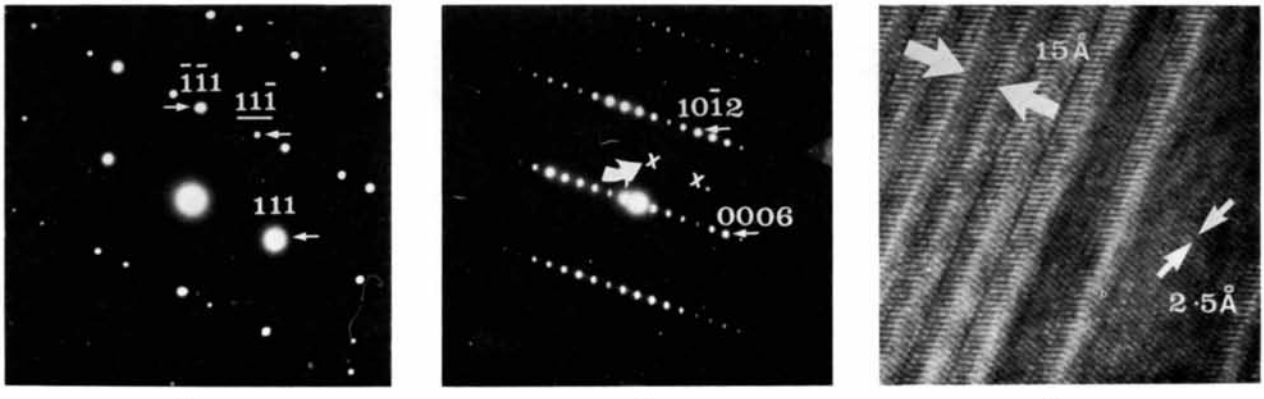

(*a*) (*b*) (*c*)

Fig. 2. (*a*) Electron diffraction pattern from a twinned crystal of the $3C$ polytype in the (110) projection. (*b*) Electron diffraction pattern from the $6H$ polytype with the incident beam in the $[1\bar{2}10]$ direction. Two alternative positions for the optic axis are marked (see § 6); that used for Fig. 2(*c*) is arrowed. (*c*) Electron micrograph showing the intergrowth of the $3C$ and $6H$ polytypes, with the incident beam tilted to place the optic axis between the 000*l* and $10\bar{1}l$ rows of $6H$ systematics to reveal the stacking sequence directly.

the stacking sequence can be represented by $[(33)_6 34]$ using Zhdanov (1945) notation. The polytype can therefore be uniquely identified as the rhombohedral $129R$ with a complete unit-cell layer sequence of $[(33)_6 34]_3$. No previous observations of this polytype appear to have been reported although Krishna & Verma (1962*a*,*b*) have observed the related $57R$ and $111R$ which have the layer sequences $[(33)_2 34]_3$ and $[(33)_5 34]_3$ respectively.

Figs. 5(*a*) and (*b*) show a small region of an apparent new short-period polytype which was found at a twin interface in cubic material. This hitherto unreported structure exists as an intermediate between the two cubic orientations. From Fig. 5(*b*), the layer sequence can be labelled *A'BCB'CAC'AB*, or in Zhdanov's (1945) notation, $[21]_3$, which would be the polytype $9R$.* This structure is of special interest in that it has a (1) in the Zhdanov symbol; the only other polytype with this symbol is $2H$ which is unstable, although known to be impurity stabilised.

* There are several possible explanations for this observed contrast behaviour, including a region of genuine $9R$, a local region of metastable structure or a *moiré* from overlapping twins. No unambiguous distinction between these possibilities has yet been made (Jepps & Page, 1979).

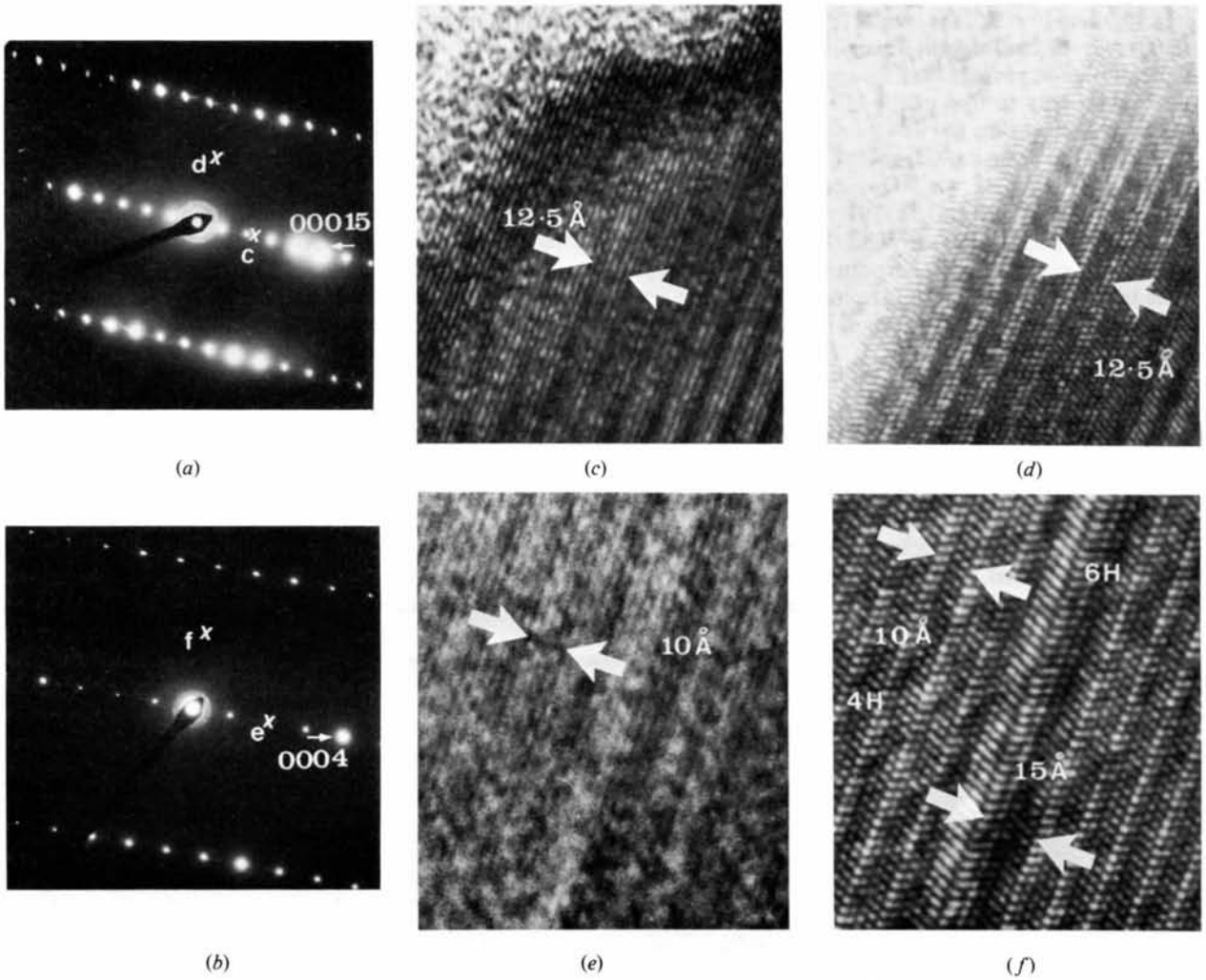

Fig. 3. (*a*) Electron diffraction pattern from the $15R$ polytype with the incident beam parallel to the $[1\bar{2}10]$ direction. Crosses mark the positions of the optic axis for (*c*) and (*d*). (*b*) Electron diffraction pattern from the $4H$ polytype with the incident beam parallel to the $[1\bar{2}10]$ direction. Crosses mark the positions of the optic axis for (*e*) and (*f*). (*c*) Lattice fringes from the $15R$ polytype with the incident beam tilted along the $000l$ row of systematics. The interlayer spacing of 2·518 Å has a five-layer modulation in the thicker parts of the crystal due to double diffraction effects. (*d*) Chevron-type lattice fringes from the $15R$ polytype with the $(23)_3$ stacking sequence clearly resolved. (*e*) (0004) lattice fringes from the $4H$ polytype, with a four-layer modulation, corresponding to the unit cell *c* dimension, imposed on the basic 2·518 Å interlayer spacing. (*f*) Chevron-type lattice fringes from the $4H$ polytype which reveal directly the expected (22) stacking sequence. A nine-layer region of $6H$ stacking is also indicated.

The region of stacking disorder shown in Fig. 6(*a*) was observed during a study of the $\beta \rightarrow \alpha$ transformation. With the incident beam tilted to a position between the $000l$ and $10\bar{1}l$ rows of systematics, the stacking sequence can be identified. There are clearly two units with the stacking (35) (again using the Zhdanov notation), which is the stacking sequence of $24R$. The area shown in Fig. 6(*b*) was observed in an extensive region of finely twinned $3C$ material. A single layer with the uncommon Zhdanov stacking symbol (1) can be seen.

6. Discussion and conclusions

It is well established that tilted-illumination lattice imaging electron microscopy techniques may be used to form images containing structural information beyond conventional microscope resolution limits. By judicious choice of both specimen orientations and beam tilts, the work reported here has demonstrated how stacking sequences in layer structures may be imaged and directly interpreted without recourse to any image or structure factor calculations based on trial structures.

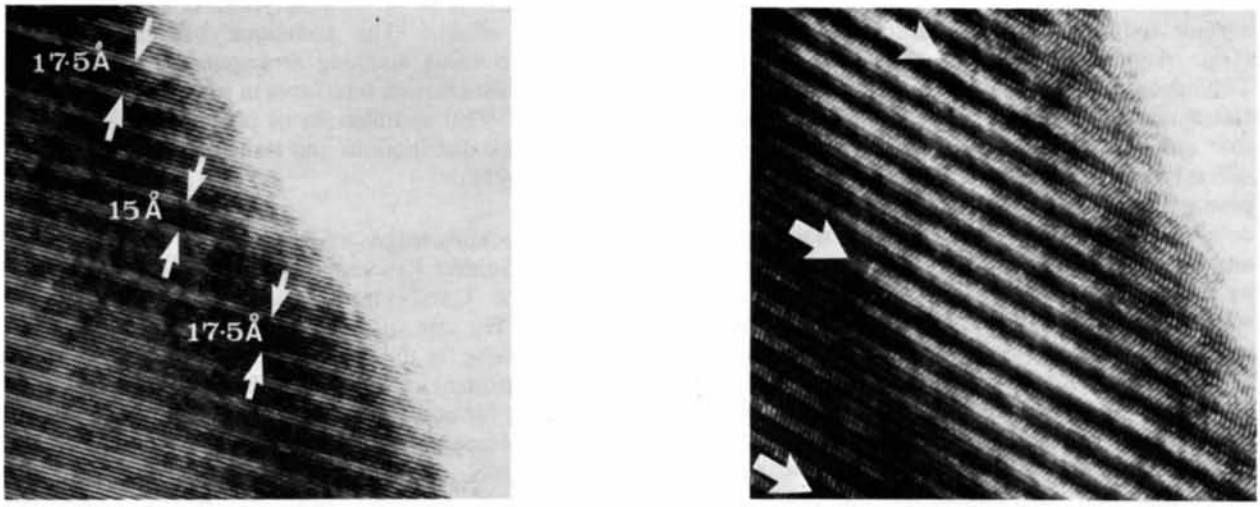

(*a*) (*b*)

Fig. 4. (*a*) Lattice fringes of 2·518 Å from the $129R$ polytype with the incident beam tilted along the $000l$ systematics row. (*b*) Chevron-type tilted-beam lattice fringes which allow the detailed stacking sequence in $129R$ to be determined directly as $\lfloor(33)_6 34\rfloor$.

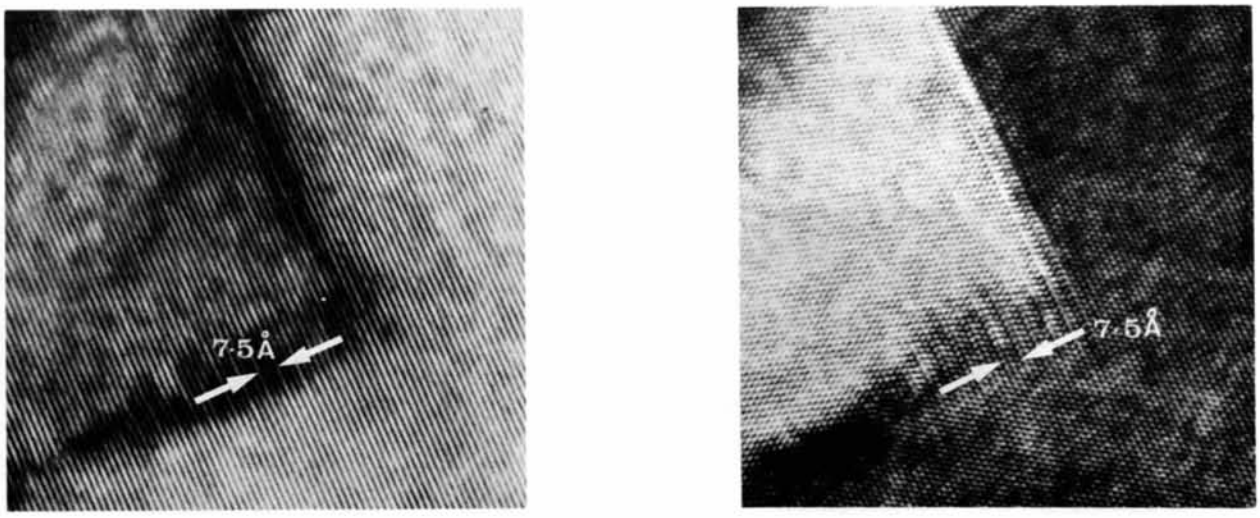

(*a*)

Fig. 5. (*a*) The tilted beam 2·518 Å (111) lattice fringes observed in the region of a $(11\bar{2})$ rotational twin interface, with a three-layer modulation superposed. (*b*) Chevron-type lattice fringes from the same area allow the stacking sequence to be identified as $(21)_3$, which corresponds to that of the polytype $9R$.

Tilted-illumination lattice imaging requires particular objective lens defocus conditions in order to form interpretable images for beams of given **g** and specific illumination and specimen orientations; through-focal series show a change in appearance with focus. However, it was found that, at the defocus positions where lattice images from these specific reflections carrying sub-unit-cell intensity modulations were sharpest, there was little relative displacement of the $10\bar{1}l$ and $10\bar{1}\bar{l}$ fringes and the fringe geometry correlated exactly with that expected from the structure/diffraction pattern. This criterion was subsequently used for the structure determination of other polytypes.

While similar resolution lattice images of silicon carbide and silicon nitride materials have been reported (Gai, Anderson & Rao, 1975; Clarke, Shaw & Thompson, 1978), polytype identification has always rested upon the number of fundamental planes within the unit-cell repeat (seen as a result of double diffraction in thicker specimen sections), *i.e.* only the primary planar stack has been resolved without any details of stacking sequences or possible structural ambiguities. Since the stack operators can be revealed by the nature of, and hence structure factor variations within, various other structural plane stacks, the current study has established the use of lattice images of specific planes to directly identify the stacking sequence.* This information is both reliable and unique regardless of either the plane stacks employed (*i.e.* regardless of the presence or systematic absence of tetrahedral face reflections), or the degree of local structural perfection. Further, in the case of crossed lattice images, interpretation of the observed contrast does not rely on the correlation of any image feature with individual atoms or groups of atoms.

Crossed lattice images, formed with reflections from the individual stacking planes together with the various inclined planes used to reveal the stack operators, may be obtained with the incident illumination tilted to place the instrument optic axis in various similar positions in the diffraction pattern such that equivalent reciprocal-lattice vectors are present in the aperture (*e.g.* the arrowed positions in Fig. 2*b*). However, different distributions of diffracted intensity may be found in the various positions yielding images of varying sharpness in terms of the relative dominance of the different sets of basal and inclined fringes. Experiment is used to determine optimum contrast in various cases.

In conclusion, it is anticipated that the techniques reported here are generally applicable to other structural problems involving polytypism or similar stacking disorder effects. The technique has already been utilized to study stacking arrangements around polytypic transformation interfaces in silicon carbide (Jepps & Page, 1979) and also forms part of a detailed study of polytype distributions and transformation mechanics (Jepps, 1979).

NWJ acknowledges a SRC research studentship and DJS the Science Research Council for financial support under the Cambridge University 600 kV HREM project. We are grateful to Professor R. W. K. Honeycombe for the provision of laboratory facilities in the Department of Metallurgy and Materials Science, especially for use of the JEM-120CX (supported by the Science Research Council). Specimens of REFEL SiC were kindly supplied by UKAEA Reactor Fuel Element Laboratories, Springfield Works. Thanks are also due to Mr S. C. Martin for the use of the structural models.

* Shaw & Thomas (1978) have recently shown that, for a particular beryllium-sialon (Be–Si–O–N), similar images agree with the structure previously deduced from X-ray data.

References

BAUMHAUER, H. (1912). *Z. Kristallogr.* **50**, 33–50.

CLARKE, D. R., SHAW, T. M. & THOMPSON, D. P. (1978). *J. Mater. Sci.* **13**, 217–219.

COWLEY, J. M. & MOODIE, A. F. (1957). *Acta Cryst.* **10**, 609–619.

(*a*) (*b*)

Fig. 6. Tilted-beam images from regions of stacking disorder: (*a*) a stacking sequence identified as $(35)_3$, which corresponds to that of the polytype $24R$; (*b*) a single layer stacking fault in a region of finely twinned $3C$ material. Locally, the structure displays the Zhdanov stacking symbol (1) (see text).

DUBEY, M. & SINGH, G. (1978). *Acta Cryst.* A**34**, 116–120.
GAI, P. L., ANDERSON, J. S. & RAO, C. N. R. (1975). *J. Phys. D*, **8**, L157–L158.
GOODMAN, P. & MOODIE, A. F. (1974). *Acta Cryst.* A**30**, 280–290.
JEPPS, N. W. (1979). Unpublished work.
JEPPS, N. W. & PAGE, T. F. (1979). *J. Microsc. (Oxford)*, **116**, 159–171.
JEPPS, N. W. & PAGE, T. F. (1979). *J. Am. Ceram. Soc.* Submitted for publication.
KRISHNA, P. & VERMA, A. R. (1962*a*). *Acta Cryst.* **15**, 383–387.
KRISHNA, P. & VERMA, A. R. (1962*b*). *Z. Kristallogr.* **117**, 1–15.
RAMSDELL, L. S. (1947). *Am. Mineral.* **32**, 64–82.
SATO, H., SHINOZAKI, S. & YESSIK, M. (1974). *J. Appl. Phys.* **45**, 1630–1634.
SAWYER, G. R. & PAGE, T. F. (1978). *J. Mater. Sci.* **13**, 885–904.
SHAFFER, P. T. B. (1969). *Acta Cryst.* B**25**, 477–488.
SHAW, T. M. & THOMAS, G. T. (1978). *Science*, **202**, 625–626.
SMITH, D. J., JEPPS, N. W. & PAGE, T. F. (1978). *J. Microsc. (Oxford)*, **114**, 1–18.
VERMA, A. R. & KRISHNA, P. (1966). *Polymorphism and Polytypism in Crystals*. New York: Wiley.
YESSIK, M., SHINOZAKI, S. & SATO, H. (1975). *Acta Cryst.* A**31**, 764–768.
ZHDANOV, G. S. (1945). *C. R. (Dokl.) Acad. Sci. URSS*, **48**, 39–42.

Acta Cryst. (1979). A**35**, 923–924

Thermal Expansion of α-NH_4HgCl_3

BY J. SADANANDAM AND S. V. SURYANARAYANA

Department of Physics, University College of Science, Osmania University, Hyderabad 500 007, *India*

(*Received* 7 *June* 1978; *accepted* 5 *June* 1979)

Abstract

α-NH_4HgCl_3 belongs to the tetragonal system with the space group P_4/mmm. Earlier X-ray studies indicate that this crystal can be described as a layer structure, the layers being perpendicular to the tetragonal axis. With a Rigaku camera, modified for work at high temperatures, the temperature variation of the lattice parameters and thermal-expansion coefficients of this crystal were determined. The coefficient of expansion, at room temperature, along the tetragonal axis is less than that in the perpendicular direction.

In this laboratory, a general programme of study of the temperature variation of the lattice parameters and thermal expansion using X-ray methods on some mixed halides of the general formula ABX_3 has been undertaken.

Ammonium trichloromercurate(II) exists in the two polymorphic forms α and β (Beljaev & Mironov, 1952). α-NH_4HgCl_3 is obtained from a melt of equimolar mixtures of NH_4Cl and $HgCl_2$. β-NH_4HgCl_3 is obtained from equimolar aqueous solutions of the same materials. The α form crystallizes in the tetragonal system with space group P_4/mmm, while the β form occurs in the orthorhombic system with space group *Pnma*.

α-NH_4HgCl_3 was prepared by heating (*ca* 523 K) a sealed glass tube containing stoichiometric quantities of mercury(II) chloride and ammonium chloride. The tube was then cooled and opened and the product ground. A comparison with ASTM data (Swanson, McMurdie, Morris & Evans, 1967) of the observed d spacings of a photograph of this sample taken at room temperature confirmed the formation of the α phase. The chemical analysis also confirmed the same, the impurities being Si, Al, Cu, Ag, Ba, Ca, Na and Mn found as traces.

Six photographs taken at different temperatures between 302 and 364 K were obtained using a Rigaku X-ray camera 114·6 mm in diameter, modified for work at high temperatures (Sadanandam & Suryanarayana, 1979). The photograph taken at about 383 K did not correspond to the one that had been obtained earlier. Above this temperature, it was observed that the colour of the sample changed from white to brown. Photographs at 383 K were repeated on more than one sample and it was confirmed that the change is of a chemical nature.

The lattice parameters were evaluated by Cohen's (1935) least-squares treatment. A comparison of the lattice parameters of α-NH_4HgCl_3 at room temperature is given in Table 1.

Table 1. *Comparison of the lattice parameters of* α-NH_4HgCl_3 *at room temperature*

a (Å)	c (Å)	Reference
4·194	7·927	Hermsen (1938)
4·1977	7·9353	Swanson *et al.* (1967)
4·1969	7·9369	Present work

0567-7394/79/060923-02$01.00